sciendo INTERNATIONAL JOURNAL ON SMART SENSING AND INTELLIGENT SYSTEMS

Article | DOI: 10.2478/ijssis-2024-0028 Issue 1 | Vol. 17 (2024)

Feasibility analysis of wireless power delivery to implanted sensors of XLIF patients

Subhas C. Mukhopadhyay[1,*], Isaac Senn[1], Vivek Ramakrishna[2], Boby George[3], Gangadhara Prusty[4], Ashish Diwan[5]

[1]School of Engineering, Macquarie University, NSW 2109, Australia

[2]University of New South Wales, Sydney, Australia

[3]Department of Medical Sciences and Technology, IIT Madras, India

[4]Department of Mechanical Engineering, University of New South Wales, Australia

[5]Department of Orthopaedic Surgery, St. George Hospital, UNSW, Australia

*E-mails: Subhas.Mukhopadhyay@mq.edu.au

Received for publication June 22, 2024.

Abstract

The paper aims to aid in developing a monitoring system for surgery patients who have undergone lumbar interbody fusion (LIF). The present body of work functions as a comprehensive analysis of relevant available literature along with our investigation regarding techniques for power delivery; both energy harvesting and wireless power transfer (WPT) alike. In addition, biological considerations are taken into account as they strongly influence the design and testing methodology of an implanted medical device (IMD). This study proposes using inductive coupling as a power delivery method. This was chosen due to the robust nature of the technology, with the IMD being deeply situated and encased in bone and tissue. Three types of receiver coil architectures were explored and designed around the geometry of a polyether ether ketone (PEEK) Extreme lateral interbody fusion (XLIF) Nuvasive Coroent XL interbody cage. With the use of off-the-shelf components, functionality was only attainable for the V3 coil design featured with 0.4 mm wire windings around horizontal and vertical beams present on the implant. The secondary coil was resonantly tuned and optimized for a 141 kHz working frequency. At a 100 mm coupling distance, it was demonstrated that a power delivery load (PDL) of 3.94 mA was able to be induced resulting in a power output of 7.21 mW. The recorded PDLs are capable of powering a high pressure P122 sensor, EFM8BB52 microcontroller, and Ultra-wideband (UWB) data telemetry link, and demonstrate the feasibility of this WPT technique for in vivo monitoring of bone fusion post XLIF surgery.

Keywords

extreme lateral interbody fusion, wireless power transfer, implanted medical device, polyether ether ketone, specific absorption rate, anterior lumbar interbody fusion, computed tomography, near field communication, polydimethylsiloxane

I. Introduction

With the aging human populace, one of the consequences faced pertains to the degeneration of the body which includes all tissues, cells, and bones. In particular, lower back pain has been attributed to be one of the leading causes of disability [1, 2]. Low back pain is such a common disorder that 70%–80% of adults will experience some form of this trauma throughout their lifetime [3]. Fortunately, most of these cases are mild in nature with 90% of injuries resolving themselves within 6 weeks [4]. However, for more severe cases of low back pain, further treatment is required.

When considering severe cases of low back pain, it is impossible to look beyond disorders such as trauma, infection, neoplasia, and degenerative pathologies; all of which can be treated through an established surgery known as lumbar interbody fusion (LIF) [5]. Through LIF, surgeons have the ability to stabilize and reinforce the problematic vertebrae which corrects spinal deformities such as lordosis; a degeneration of the spine whereby the vertebrae curve inwards excessively [1]. Research undertaken by Martin et al. [7] determined that in 2015, 79.8 per 100,000 Americans were undergoing LIF which comes with significant medical expenses in excess of 50,000 USD [6]. Alongside personal economic detriment, companies also face significant losses with low back pain being highlighted as the most frequent cause of absenteeism from the workplace.

In simple terms, LIF can be likened to a welding process, whereby problematic vertebrae are fused to form a single, solid bone [5]. The theory behind this process was established by Briggs and Milligan [8] in 1944 and centered around the notion that restricting the motion of the painful vertebrae will result in reduced pain, and decompression of any pinched nerves. In order to accomplish this, the treatment process involves the replacement of a problematic intervertebral disk with an insertion known as an interbody cage. If necessary, further securement of the implant may be done so using metallic instrumentation in the form of rods and screws which are affixed to the vertebrae. Pockets in the interbody cage are filled with material used to promote bone growth to ensure the vertebrae are joined together [1].

Approaches to LIF surgery typically revolve around a best-case scenario for both the patient and surgeon; according to the general criterion of minimally invasive surgery, reduced postoperative pain, and quicker returns to everyday life [5]. Although once thought to be best supported through anterior lumbar interbody fusion (ALIF), Ozgur et al. [9] determined that their novel surgical application of extreme lateral interbody fusion (XLIF) was the ideal solution. Compared to ALIF that provides spinal access through the abdomen, XLIF approaches the spine through the side of the body along the flank region below the rib cage. This allows the interbody cage to be delivered without manipulation of the spinal cord or surrounding large vessels [1, 9]. Furthermore, this method of surgery allows for the implantation of an interbody cage with the largest footprint [10]. Thus, providing the greatest level of flexibility when the inclusion of embedded hardware in the implant is considered. Figure 1 demonstrates the potential LIF surgery types and their relevant access points. Typical LIF implants are constructed from titanium or

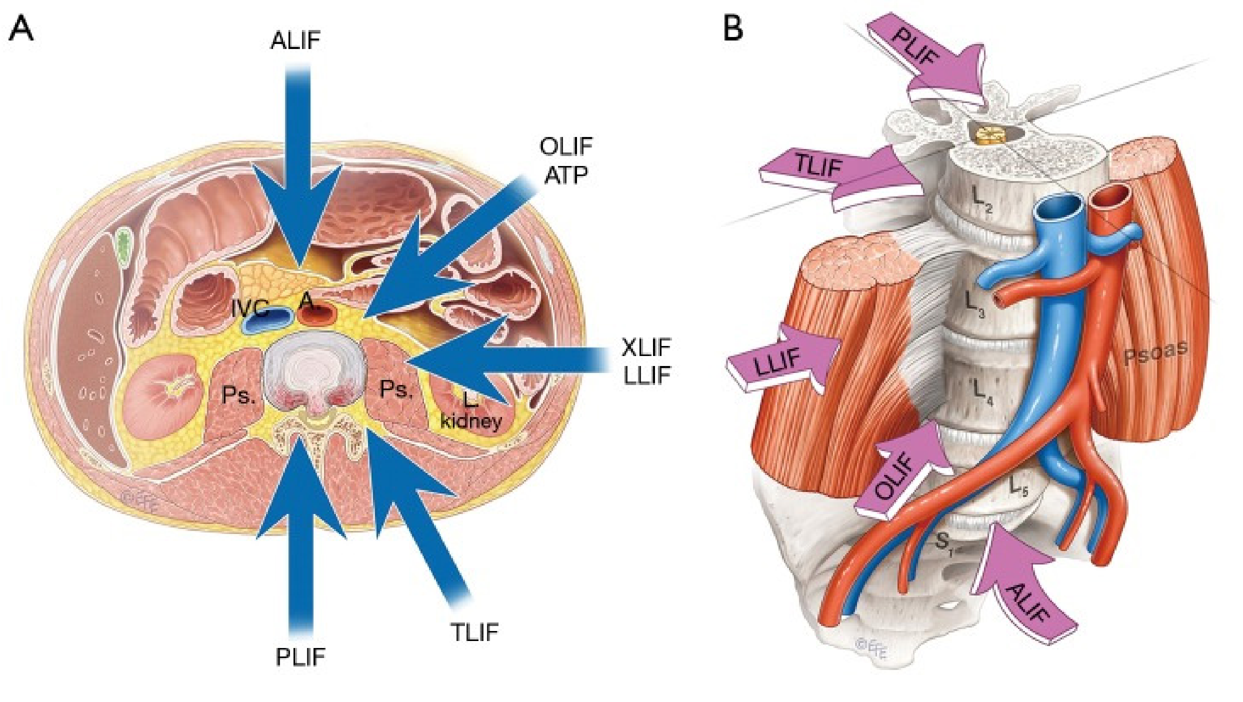

Figure 1: A. Cross-sectional view, B. Normal view. LIF surgery types and their relevant access points [1]. LIF, lumbar interbody fusion.

polyether ether ketone (PEEK); however, in the context of this project, the latter was chosen due to its availability, cost, and electrically insulative properties [11]. In particular, the conductive nature of titanium was avoided as it may have the chance to interfere with sensor measurements, wireless data transmission, and wireless power transfer (WPT) [12].

While there exist several complications that can arise due to LIF surgery including subsidence [13], screw loosening [14], and screw breakage [15]; this project focuses on the development of an implanted medical device (IMD) capable of monitoring for pseudarthrosis. Pseudarthrosis refers to the incomplete bony fusion of the targeted vertebrae and typically manifests with pain lasting for months to years after the initial operation [16]. Following LIF, rates of pseudarthrosis range in the region of 5%–35%, with success rates being much lower in those who have undergone fusion spanning three or more levels, or those who have poor bone quality [17]. Additional underlying risk factors that affect the outcome of bony fusion are cited to be lifestyle-related such as alcoholism, smoking, and malnutrition [16] as well as surgery-related such as interbody cage material [18] and bone graft material [19]. Considering the multitude of factors that may affect the outcome of LIF, it is essential to have a method through which progress can be monitored. Or else, surgery is required for a second attempt at bony fusion [16].

Current monitoring techniques utilized by surgeons revolve around imaging methods such as plain radiographs and fine-cut computed tomography (CT) scans. However, in the case of plain radiographs, the approach has been shown to follow no clear standard and is deemed ineffective at detecting pseudarthrosis [20]. Furthermore, CT scans have been cited as returning high false-positive results when assessing bony fusion [21]. Hence, an alternate technique for patient monitoring post-LIF surgery is necessary.

For fully functioning IMDs, there remain a few criteria that must be achieved. These relate to the implementation of a sensor, control circuit, and both a power and communication protocol. If these elements are not present, then the circuitry designed is not suitable for IMD use [22]. Thus, the scope of this project is related to exploring the methods through which power delivery can be realized for use in an IMD to be utilized for those who have undergone LIF. Further research included the details of the techniques for sensor data extraction. Additionally, all research that are undertaken must consider industry standards and biocompatibility, ensuring adverse effects are not experienced [23-36].

Due to the deep-situated nature of the interbody cage, wired *in vivo* monitoring is not feasible and the project must use an IMD. Additionally, there remains a lack of methodology surrounding the detection of pseudarthrosis which further highlights the requirement for a monitoring system. Current literature typically revolves around IMDs surrounded by soft tissue, except for neurostimulators that are shallowly implanted. Hence, research are undertaken to determine the effects of both hard and soft tissue attenuation of power delivery to a deeply (up to 12 cm) located IMD [38-46].

II. Considerations of IMDS for Wireless Power Delivery

a. Data transmission

Typically, backscattering is used for passive backward data telemetry in inductive coupling links. This technique does not require an active antenna, which minimizes power consumption on the implant side. The most widely used method of backscattering is load shift keying (LSK), whereby the load connected to the secondary side is modulated by shorting the resonant tuning LC tank [80]. A major requirement for this method is a high coupling threshold, as defined by the mutual inductance between the two coils. Furthermore, LSK represents a source of power loss when the resonant capacitor is shorted [81]. When shorting occurs, the connected DC rectifier is starved of power and does not continue to provide power to the attached DC load. As such, more complex circuitry is required in the form of a battery which can maintain a required level of power to the load while LSK is employed [49, 53, 56-61].

In cases, where LSK is not a viable means due to the low coupling factor, active antennas are required instead. Ultra-wideband (UWB) is a short-range wireless communication protocol that has shown to be the most promising when considering low power requirements and mm-sized componentry [80]. Two examples in literature utilized UWB antennas and can transmit data at a 67 Mbps rate across 1–10 cm with a 1.2 V power supply and 1.833 mA of current [82]. The second example was able to achieve a 100 Mbps rate across 1–400 cm with the help of an amplifying horn and required a similar 1.2 V power supply, but only 1.675 mA of current [83].

b. Biological tissue damage

In the scope of WPT and IMD use, tissue damage can occur due to two main reasons. These are (a) inflammatory response [84] and (b) heat damage [85]. Inflammation is best described as the process by which vascular tissue reacts to localized injury. In the case of IMDs, the surgical procedure commences a bodily response where mechanisms are activated in an attempt to maintain homeostasis. In particular, Anderson [84] notes that the acute and chronic inflammatory response alongside foreign body reaction to the formation of granulation tissue all prevent the healing of a wound and present an issue. Since Anderson's research in 1988, further research has been conducted regarding the biocompatibility of implant materials. Recent literature suggests that the biological response can be reduced with the replacement of hard materials with soft materials that match the tissue stiffness at the site of implantation [62].

In addition to an inflammatory response to IMD insertion, WPT techniques impart energy onto tissue resulting in heating. The measure of volume relating to heating caused by the impart of electromagnetic energy is known as the specific absorption rate (SAR) and must be considered [85]. Furthermore, inefficiencies in implant circuit design can also result in component heating, which is conductively transferred to surrounding tissue. It is essential to ensure that tissue temperature does not rise by more than a few degrees, as this is the point at which protein denaturation occurs [37, 85]. Davies et al. [86] explored the heat effect of an implanted medical heart and found that with a temperature increase of 1.8°C, a fibrous capsule with increased capillary density developed surrounding the implant over a period of 7 weeks. However, these results were not permanent and naturally resolved themselves over time. Overall, the temperature raise did not result in adverse effects when staying under the 2°C recommended limit [63-79].

c. Implant biocompatibility

To ensure the durability of the sensor, it is necessary to encase any open electronics in a material that will prevent them from being damaged. This is especially important in the case of IMDs, where human mobility would result in constant shifting of the components. Furthermore, IMD components, such as the range of PZT piezoelectric materials, are toxic and require encapsulation [87]. When considering the need for component encasement, an equally important factor is the requirement for the encasing material to be biocompatible; meaning that the surrounding tissue will not experience any long-term adverse effects due to the implant [88]. Additionally, strong adhesion between the target tissue and implant must be feasible, as this remains a critical requirement for stable IMD performance [87]. Special consideration must be taken as instant adhesion is considerably more difficult when wet surfaces such as body tissue are involved.

Laube et al. [89] determined that silicone alone cannot create a hermetic seal around electronics. Instead, components first needed to be coated in parylene C which has negligible permeability, high adhesion to silicon, and *in vivo* biocompatibility. This is further supported by Zhuang et al. [90], who concluded that silicon without an additional compound was unstable in long-term IMD applications. In their project, parylene C was used which resulted in increased longevity of insulation in harsh, aqueous environments. The authors additionally tested the use of polydimethylsiloxane (PDMS); however, results remained inconclusive for this compound. In comparison, Lee et al. [91] conducted intensive testing between both parylene C and PDMS coated implanted *in vivo* in rats for a period of 12 weeks and determined that parylene C resulted in greater biocompatibility, with a reduced immune response. Despite this, PDMS also presented itself as a viable option and it had excellent biocompatibility [92, 93].

III. Performance Analysis of WPT

This section defines the method of approach and measures of success, as well as the IMD power requirements.

a. Approach

As this research focuses on the feasibility of WPT for deep IMDs encased in bone and tissue, a finalized product is not the goal of this project. Rather, the methodology and results aim to explore if it is possible to transmit reasonable amounts of power over long distances. High-level concepts relating to optimization are not explored, and primarily off-the-shelf components are utilized [101].

Testing is conducted to determine the effect of the following measures of misalignment; being (a) vertical, and (d) angular. A visual representation is provided in Figure 2, which demonstrates each form of misalignment.

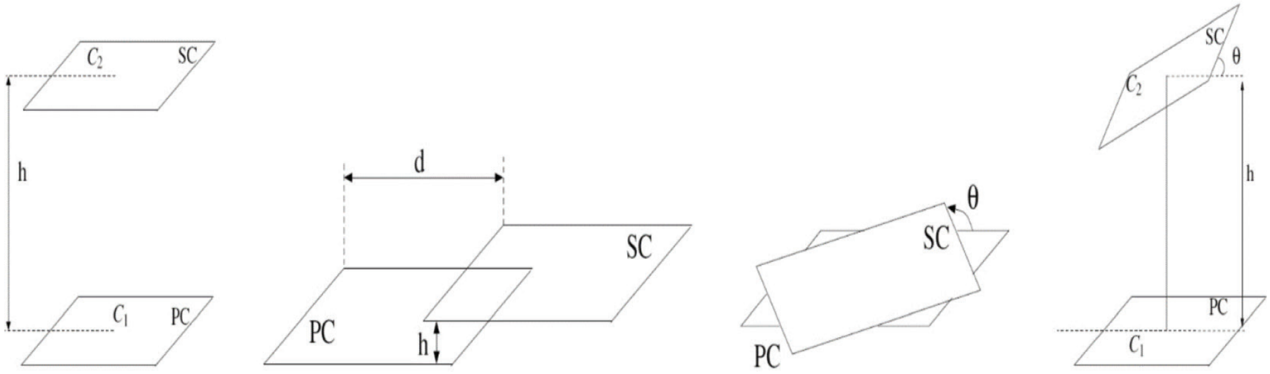

Figure 2: Vertical, horizontal, planar, and angular misalignment [113].

b. Measures of success

The following items are measures of success, which require unanimous satisfaction when considering the feasibility of an inductive coupling power delivery system for *in vivo* XLIF patients.

1. Coil dimensions must not increase implant dimensions by >1 mm in each direction.
2. Coil temperature must not rise by >1.5°C while being powered.
3. Coupling distances in XLIF patients vary, requiring WPT to function across a 40–100 mm range.
4. At the maximum range (100 mm) a minimum of 1.8 V is necessary for the EFM8BB52.
5. At the maximum range (100 mm) a minimum of 1.9 mA is necessary if LSK can be employed, else 3.8 mA is required.

c. IMD power requirements

c.i. Microcontroller

Representing an unoptimized solution, the current hardware employed which features successive approximation ADC is the EFM8BB52 microcontroller developed by Silicon Labs [94]. When operating at an ambient temperature of 25°C with a 1.8 V supply voltage (V_{VDD}), the Table 1 represents typical supply current consumption. The decision to utilize an external voltage reference for ADC was done so as to using V_{VDD} as the reference voltage (V_{VDDREF}) requires a voltage divider that consumed 16 µA in comparison to the 5 µA of $I_{EXTVREF}$. Additionally, there exists an integrated temperature sensor with a supply current consumption of 50 µA (I_{TSENSE}). However, in an effort to save power, this hardware element can be disabled.

Table 1: EFM8BB52 microcontroller component current requirements [94].

Parameter	Symbol	Typ	Unit
Normal mode at 80 kHz using low-frequency oscillator	I_{NORMAL}	612	µA
ADC supply current at full speed with 12-bit conversions	I_{ADC}	250	µA
External voltage reference input current	$I_{EXTVREF}$	5	µA
Current for VDD divider when VDD used as VREF	I_{VDDRED}	16	µA

c.ii. Piezoresistive pressure sensor

The piezoresistive sensors used for pressure sensing are the P122 High Silicon Pressure Sensor Die developed by Amphenol Sensors [95] as shown in Figure 3. When excited with a 1 mA input, the sensor will produce an output that is proportional to the pressure exerted upon the die. For full scale output, a minimum voltage supply of 320 mV is required. Although there exist seven P122 sensors on the piezoresistive sensor array, it is not necessary to power all components simultaneously.

c.iii. Data transmission

While not currently realized in this project, data must be able to be transmitted wirelessly back to the user for real-time analysis of the fusion process. LSK is a means of backscatter that allows data to

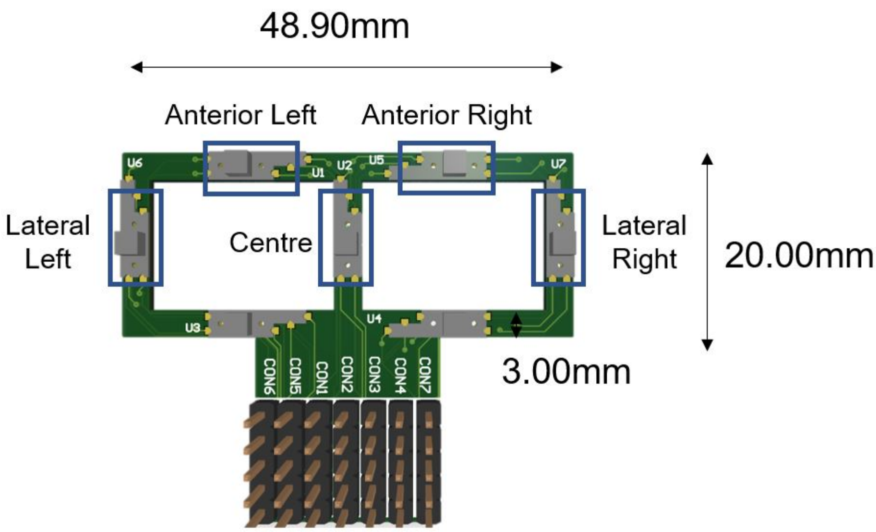

Figure 3: Piezoresistive sensor array.

be transmitted back to the primary coil by shorting the secondary capacitive tank. Analysis of this technique allows for data transmission without the use of extra components which would require powering. If LSK is determined to be infeasible for this project, active components will be necessary for data transmission. UWB is the most promising technology for this, and it has been shown that data has been transferred using millimeter-size components across centimeter distances. Two examples in literature have transferred data across 10 cm, requiring a 1.2 V power supply and 1.675 mA [83] or 1.833 mA [82]. As such, the summation of all considered elements is 1.867 mA if LSK can be utilized, or 3.7 mA if active data transmission hardware is necessary [110, 111].

IV. System Design and Results

a. Coil design

To demonstrate the ability of the off-shelf components, two commercially available transmitting inductive coupling modules were purchased. It is important to note that this research focuses on the feasibility of using WPT for deep-situated IMDs, and that the components purchased are not representative of the most optimized inductive coupling transmitting coil designs.

a.i. Transmitting coil module

With the module developed by the same company, the high power transmission circuit also makes use of two ICs created by Taidecent—the XKT-801 and XKT-1511, as shown in Figure 4.

a.ii. Receiver coil design

Arising from complexities in the geometry of the screwed interbody cage design as shown in Figure 5, it was not possible to wrap coils around the horizontal beams of the implant. Rather, coils could only be wrapped around one external vertical beam and internal vertical beam. Following the formula for self-inductance Eq. (1), a reduction in turns results in drastically lower inductance. Ultimately, affecting the mutual inductance between the transmitter and receiver Eq. (2). Hence, this project focuses on the feasibility analysis for the standalone implant architecture before exploring coil architectures for the screwed variant.

Self-inductance:

$$L = \frac{N^2 \mu_r \mu_0 A}{l} \tag{1}$$

Mutual inductance:

$$M = k\sqrt{L_1 L_2} \tag{2}$$

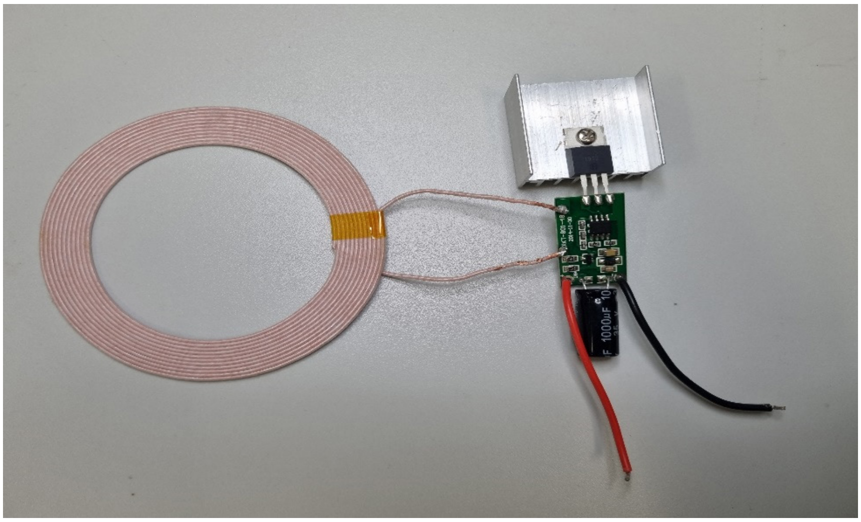

Figure 4: High power transmitting coil and circuitry.

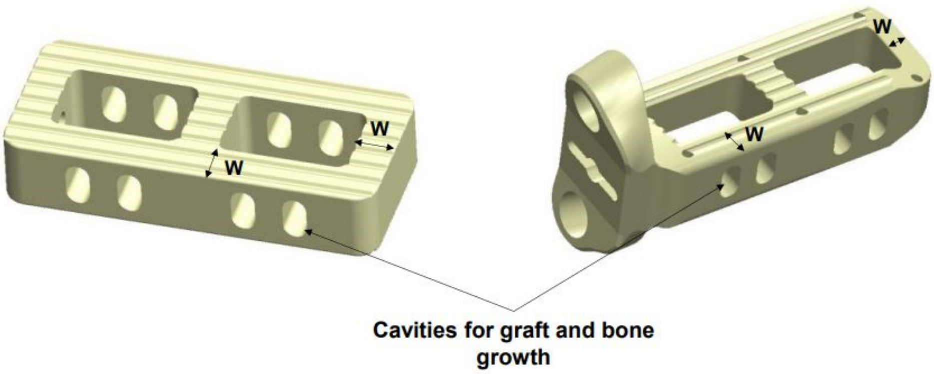

Figure 5: Implant standalone version (left) and screwed version (right) [96].

Initial receiver coil designs were developed around a prototype created that mirrored the architecture of the commercially available PEEK interbody cage Coroent XL developed by NuVasive [96]. As explained earlier, for the purpose of feasibility analysis, preliminary receiver coil architectures were created around the standalone design seen in Figure 5.

Using the dimensions of the interbody implant, a CAD model was developed in Creo Parametric [97] to assist with the hand-winding of coils. The design featured extrusions which guided the positioning of the wire. Only minor changes were made in an attempt to mirror the original implant dimensions as closely as possible [112].

To create the coils, the coil winding helper was fastened in place with a clamp and manually wound using 0.4 mm copper enamel-coated wire. Wire of this diameter was chosen due to three reasons:

- Commercial availability.
- Success measure 1—the width added to the dimensions of implant due to the coil stay within the constraints.
- Simplicity—a large wire diameter results in less coils and easier manufacturing.

The three coil architectures can be seen in Figure 6. The added complexity of V2 and V3 significantly impacted the manufacturing time with the V3 coil requiring 60 min of winding time compared to 15 min for V1, and 45 min for V2. Unfortunately for the experimental results, only the V3 coil resulted in reasonable levels of induced power. As such results from the other two coils will not be mentioned.

While not ideal, dependent on the results conducted in the vertical misalignment experiments, copper enamel-coated wire with a diameter of 0.25 mm also represents a suitable choice for coil material. A wire of this dimension would allow for an almost four-fold increase in coil turns if a multilayer design was employed, resulting in a greater self-inductance despite the increased coil length Eq. (1).

Consulting the American Wire Gage Conductor Size table for copper, it can be observed that 22 gage wire (consisting of a 0.254 mm diameter), has the maximum current carrying capabilities of 0.92 A. Following the current requirements outlined in success measure 5, this proves to be a suitable wire choice if necessary.

b. Experimental results

b.i. Vertical misalignment analysis

Vertical misalignment refers to the vertical spacing between the primary and secondary coils. When the two coils are perfectly aligned with no misalignment, the coupling factor and mutual inductance have the highest efficiency [52]. From the point of origin, magnetic waves undergo attenuation when propagating through any medium, with the magnetic permeability of the medium influencing this factor [48, 51]. As such, the effects of vertical misalignment must be explored to understand the capabilities of the transmitting coil.

Practical analysis for the vertical misalignment experiments was conducted using the setup seen in Figure 7. The transmitting coil was affixed to the elevated wooden beam using a fishing line, and the coupling distance between the receiver and the transmitter was varied with a scissor jack. Due to the metallic composition of the scissor jack, a wooden spacer was placed between the receiver coil and the scissor jack plate to ensure no interference with the magnetic field. Vertical adjustments were made by turning the knob attached to the scissor jack.

As demonstrated in literature [52], inductive coupling WPT is most efficient when resonant coupling is employed. When the secondary coil loosely resonates at the frequency of the wavelength, the coupling factor increases in strength. This technique requires integrating the optimal receiver LC circuit as explored below.

Using the Rigol DS1054Z Oscilloscope [98], it was seen that the working frequency of the high-power transmitting coil was 141 kHz with an average time period of 7.09 μs. It is unknown how the

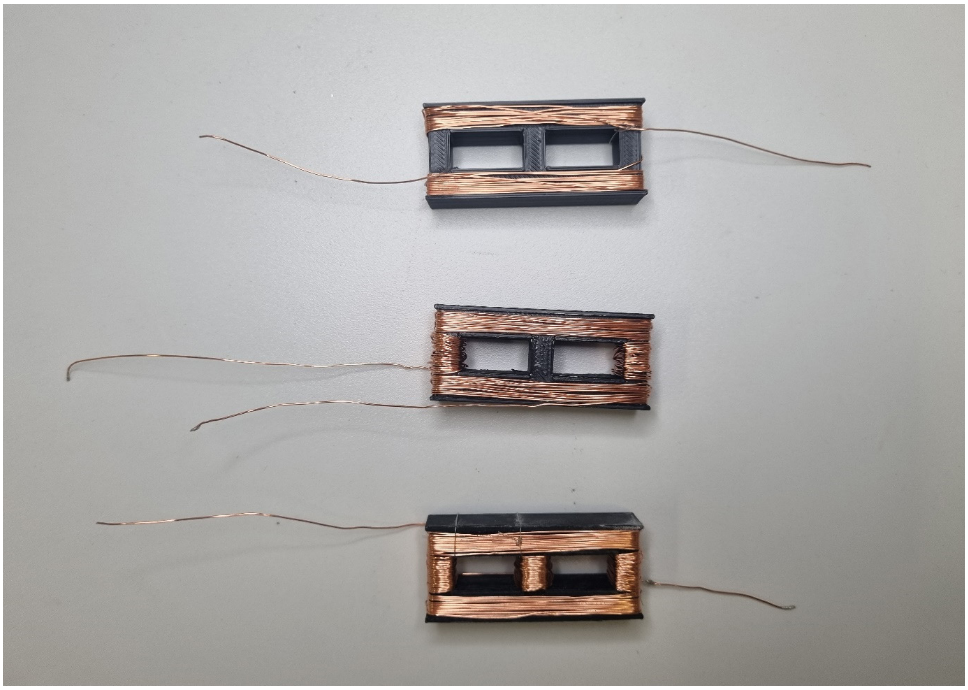

Figure 6: Coil V1, V2, and V3 designs using standalone implant geometry.

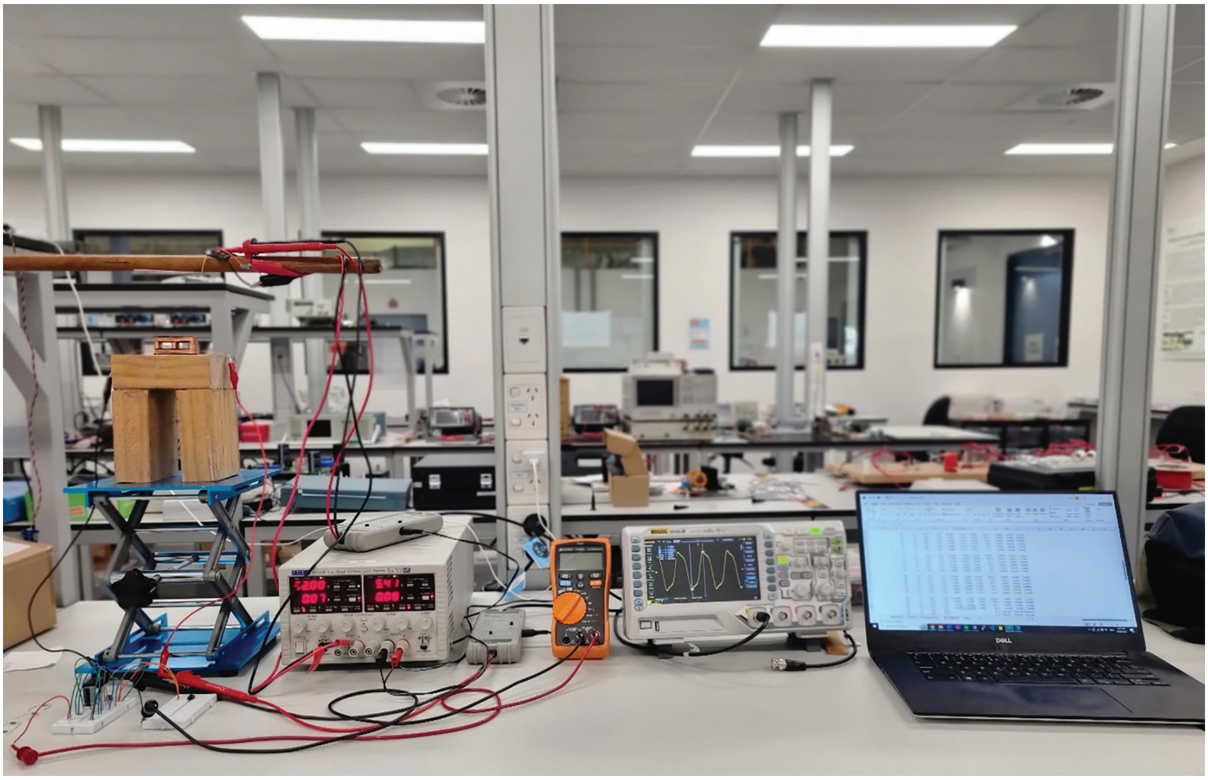

Figure 7: Vertical misalignment testing setup.

working frequency is dictated, and a discussion with the IC manufacturer, Taidacent, yielded no results. The inductance of the coils was measured using a Keysight U1731C handheld LCR meter [99]. The following formula can be used to determine the necessary capacitor value for the LC circuit.

$$\omega_0 = 2\pi f_0 = \frac{1}{\sqrt{LC}};\ f_0 = \frac{1}{T_0}$$

$$\therefore C = \frac{T_0^{\ 2}}{4\pi^2 L} = \frac{1}{4\pi^2 f_0^{\ 2} L} \tag{3}$$

In an attempt to offset the instantaneous forward voltage drop introduced with rectifying diodes, testing was conducted using Schottky IN5822 diodes from Onsemi [100]. For instantaneous forward current values of 50 mA and below at 25°C, each Schottky diode exhibits only a 0.22 V forward voltage drop. For minimum forward voltage drop, a half wave rectifier circuit was implemented using the IN5822 and a large smoothing capacitor. The circuit can be seen in Figure 8.

At varying heights, by varying loads, the voltage and current levels were tested with a half-wave Schottky diode bridge rectifier. It was determined that to meet success measure 4 and 5, a 463.8 Ω was ideal, as demonstrated in Figure 9. At 100 mm, 1.828 V and 3.941 mA were achieved. While the minimum voltage was achieved at later distances using a smaller DC load, the induced current was not sufficient for powering of an active antenna.

b.ii. Angular misalignment analysis

Inductive links have the tightest coupling factor when the primary and secondary coils are parallel to one another, with no angular, planar, or horizontal misalignment present. Due to the vertebral alignment of the spine, natural angle is introduced and results in angular misalignment if the transmitting coil is held parallel to the back region. Figure 10 demonstrates the natural curve of the spine, along with spinal deformities which XLIF aims to provide relief from [1].

Utilizing the same testing setup outlined before, the effects of angular misalignment were explored across the 40–120 mm range at 20 mm intervals as shown in Figure 11. The primary coil was attached to a dowel constructed from wood and was rotated clockwise along specified angles the range of 0–90°, with 90° being perpendicular to the receiving coil.

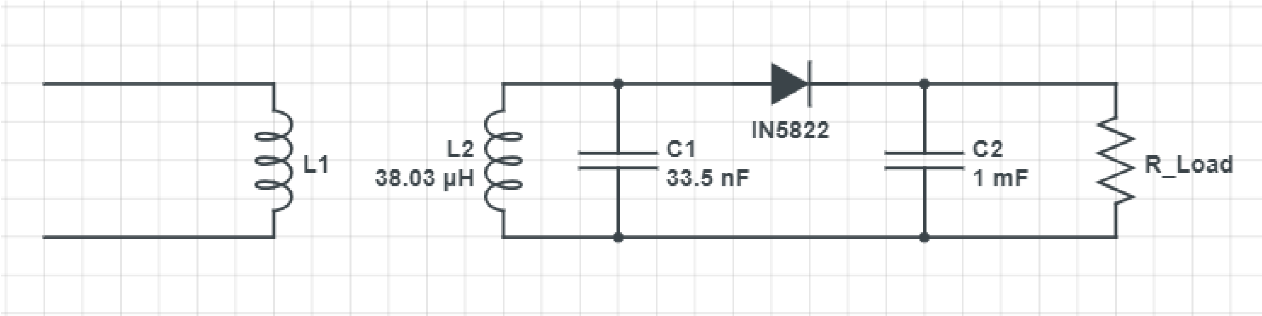

Figure 8: Half-bridge receiver perfectly tuned for 0.4 mm standalone v3 coil.

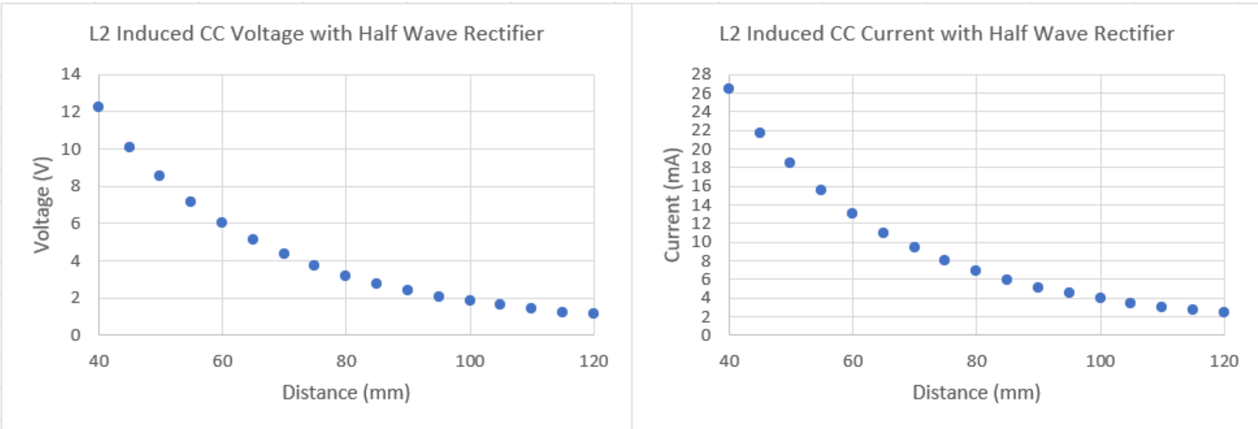

Figure 9: Receiver half-bridge distant dependent CC results through air.

The transmitting circuit uses the high-power transmitting coil provided with 32 V, and the receiving circuit makes use of a Schottky diode half wave rectifier. The DC load connected to the filtered rectified output was 463.8 Ω.

Table 2 demonstrates the losses in PTE and power delivery load (PDL) at varying misalignments and distances in reference to the baseline 0° values, whereby the two coils are perfectly aligned in a parallel manner.

Angular misalignment results in greater WPT disruption when comparing CC values. Thus, it would be preferable for the patient, or doctor, to rotate the transmitting coil to be parallel with the interbody cage. In doing so, it is important to note that reducing angular misalignment results in a greater level of vertical misalignment [114-116, 120].

While there have been inductive coupling receiver architectures designed which limit the effects of angular misalignment [54, 55], these systems are not suitable for the project as the designs necessitate coils traveling along all three-dimensional planes. As necessitated by success measure 1, increasing the implant size with further coils is not a feasible solution. A reduction in wire size would facilitate a 3D receiver coil architecture but would require timely manufacturing methodology. Rather, it is suggested that a more optimized transmitter coil and transmitter circuit design is employed.

Considering the fact that the current unoptimized equipment meets the minimum threshold defined by feasibility success measure 4 and 5, angular misalignment is not an element that can be present in the system. As suggested, when designing the optimized primary coil, it is essential that an 'overhead' is implemented, whereby the transmitting coil is able to be rotated by a reasonable degree while still providing the necessary power to the IMD.

b.iii. Tissue attenuation analysis

As the scope of the project revolves around the creation of an *in vivo* biomedical implant, it is essential for

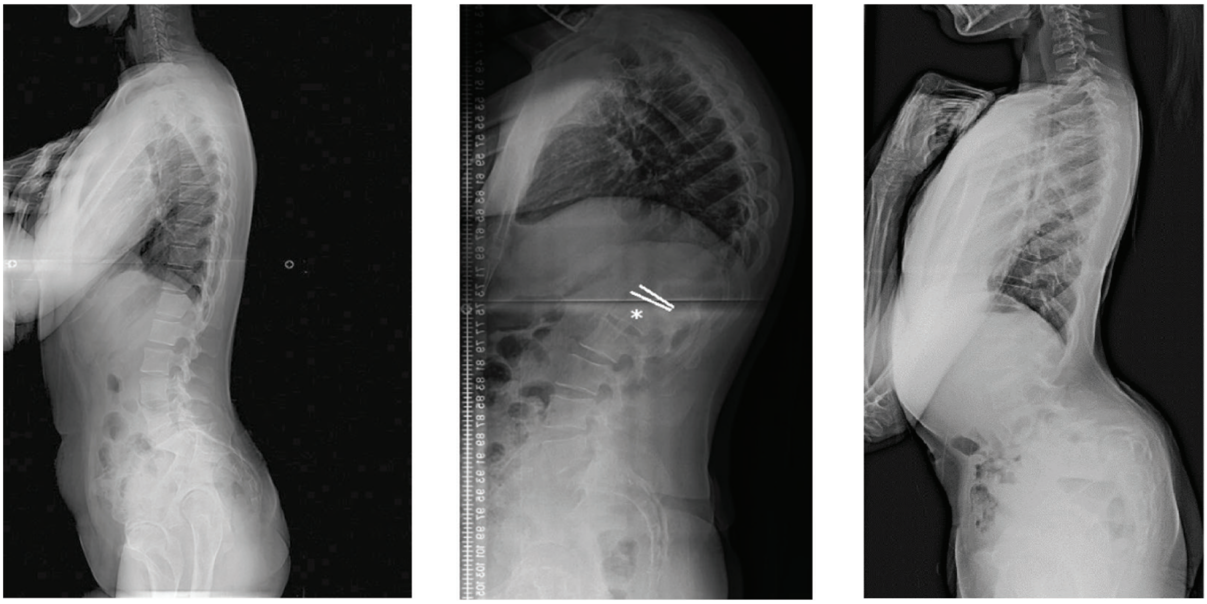

Figure 10: X-ray of a natural spine [119], kyphosis [118], and lordosis [117].

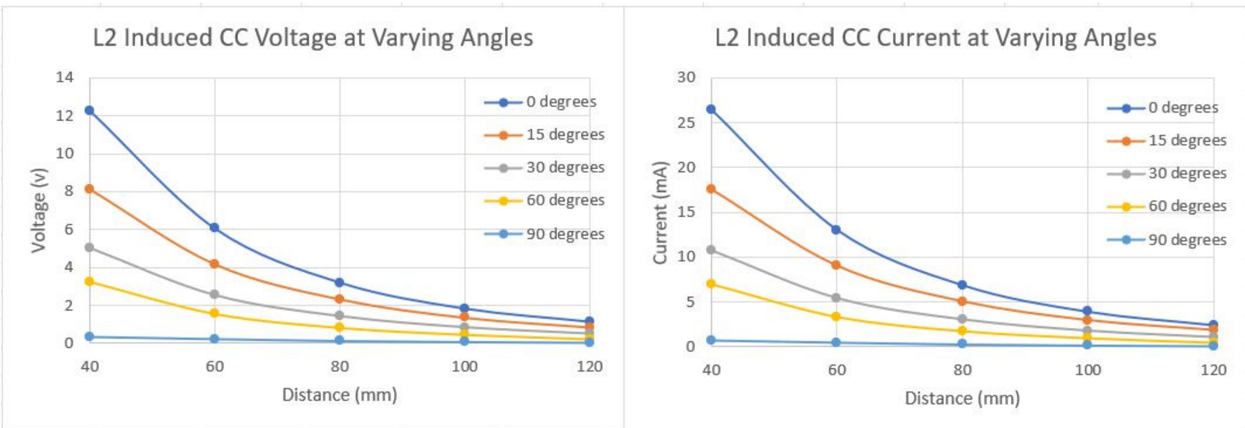

Figure 11: Receiver CC results at different distances and angles.

Table 2: PTE and PDL losses due to angular misalignment.

Misalignment (°)	Loss in PTE (%)	Loss in PDL (%)
0	0	0
15	24–34	24–34
30	56–59	56–59
60	74–81	74–81
90	95–97	95–97

PDL, power delivery load.

testing to be conducted through the medium of tissue substitutes to determine whether the biomechanical properties of the body affect the propagation of magnetic waves.

To simulate adipose and muscular tissue, chicken breast was used. In addition, there were two synthetic bone mediums developed by Sawbones [102] which were created to mimic the mechanical properties of human bone. The synthetic vertebrae consisted of a 0.3 mm layer of cortical bone and a 5 mm layer of cancellous bone. Cortical bone is the hard compact type of bone found on the outer layer of long bones, with a typical 0.3 mm shell seen on vertebrae in the lumbar spine [103]. The width of cancellous bone was determined based on the average dimension (29.7 mm) of the lumbar intervertebral disk [104].

Although substitutes for tendon were not integrated into the phantom tissue design, the three mediums chosen represented a tissue design from which assumptions could be formed. Figure 12 demonstrates the tissue substitutes, forming a 120 mm vertical misalignment between the two coils.

Closed circuit tests were conducted three times and averaged at distances of 40 mm, 80 mm, and 120 mm with varying loads as outlined in the closed circuit results through air. A slight variance was observed in the closed circuit voltage measurements but can be attributed to a small shift in the transmission position when contact was made between the coil and the silicone rubber. Overall, negligible differences were observed when comparing Figure 13 with Figure 11.

It is seen that reducing the frequency at which the secondary coil resonates will provide PDL gains; however, at the expense of PTE [52]. As the perfectly tuned circuit is only capable of providing 1.8 V at 100 mm, it is not possible to reduce PTE. It is crucial to note that increasing PTE should remain a major focus on any further project developments as a lack of efficiency indicates heat dissipation in coils, tissue exposure to AC magnetic field, and interference with nearby electronics [50, 51, 47]. Furthermore, it is not recommended to reduce PTE in favor of increasing PDL as the current capabilities at 100 mm are already sufficient for the project following success measures 4 and 5.

For both the preliminary and secondary receiver circuits, a 1000 μF capacitor was chosen for the smoothing filter because a capacitor of this value highly minimizes DC voltage ripple. It is to be noted that the form factor of this capacitor is quite large, and in the context of an IMD where miniaturization is required, does not represent the optimal solution. This project limitation must be explored to determine the maximum allowable level of voltage ripple while still meeting the measures of success.

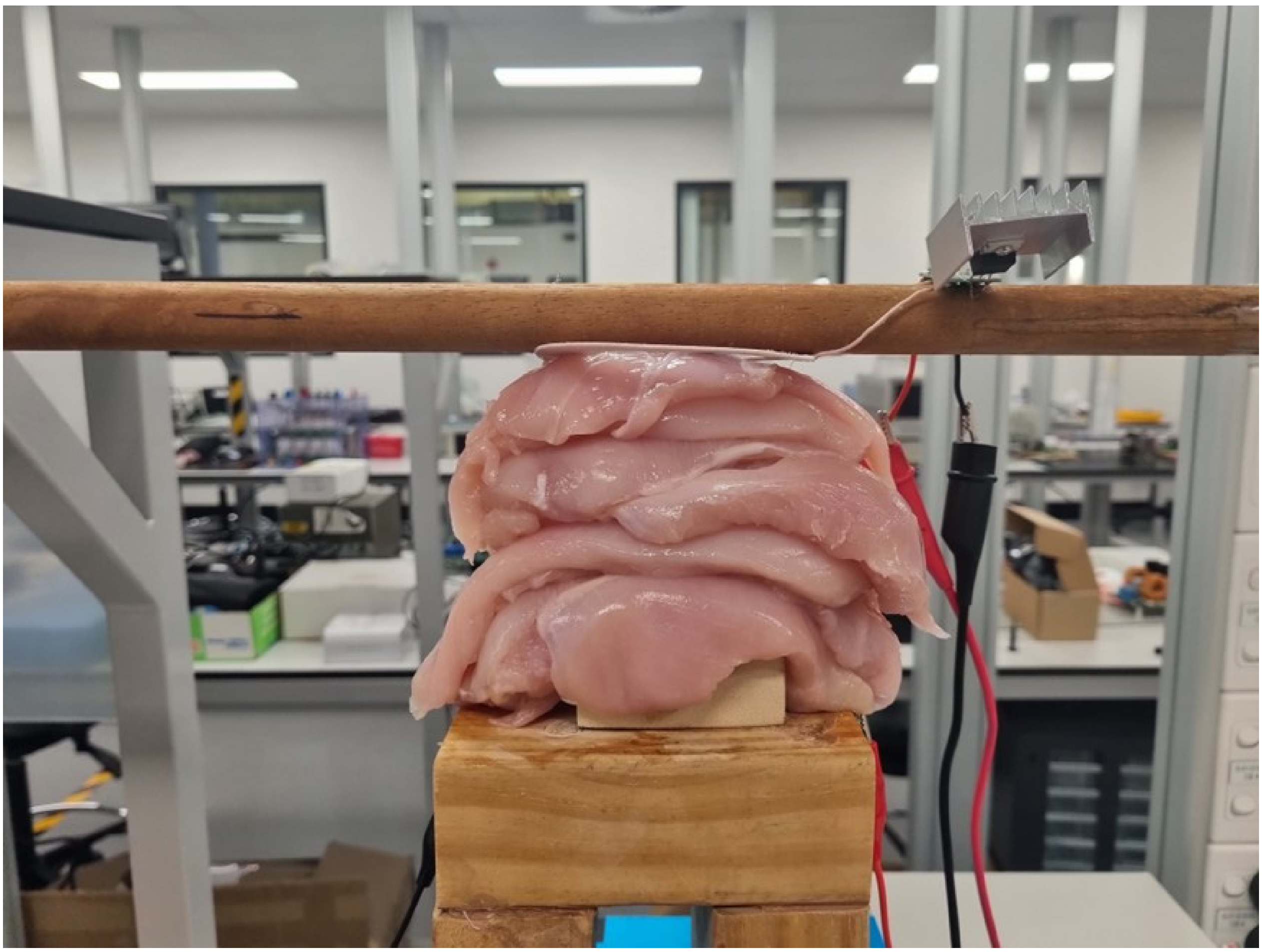

Figure 12: Vertical misalignment testing setup using tissue substitutes.

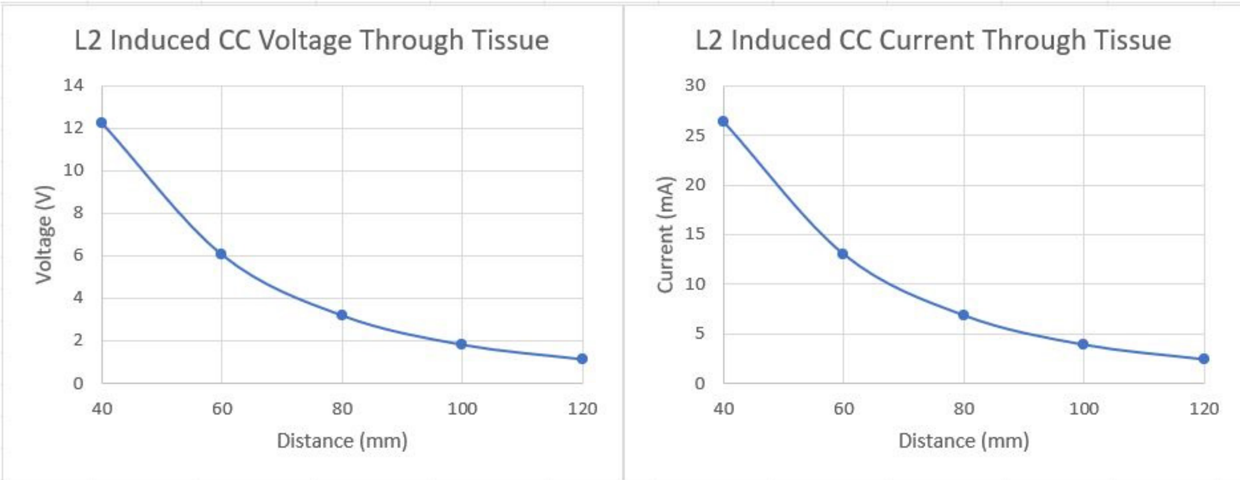

Figure 13: Receiver CC results at different distances through tissue.

Regarding AC to DC voltage rectification, we must highlight the importance of developing a circuit that features minimal voltage drop. When observing the results from the experiments, using the IN5822 Schottky diode which featured a 0.22 V forward voltage drop, it is observed that the maximum powering distance is 100 mm when considering the same factors for success. Further optimized methods of rectification should be explored to optimize the PTE and PDL across the DC load on the secondary coil.

b.iv. Receiver coil temperature analysis

Temperature measurements were taken using a commercially available, low cost, high accuracy TMP117 sensor developed by Texas Instruments [105]. Presenting itself as the ideal solution for this analysis, the TMP117 provides 16-bit resolution with an accuracy of ±0.1°C across the range of –20°C to 50°C with no calibration. Electronics company Core Electronics [106] integrated the sensor in a package that allows for simple connectivity between the TMP117 sensor and a Raspberry Pi using the I2C data transfer protocol programmed in Python version 3+ [107].

Direct contact was made between the TMP117 and the receiving 0.4 mm standalone V3 coil under the following test conditions:

- High power transmitter operating at 32 V and 0.07 A
- 40 mm vertical misalignment
- 0 mm horizontal misalignment
- 0° planar misalignment
- 0° angular misalignment
- 463.8 Ω DC load

In these conditions, the receiver coil outputted 12.26 V and 26.43 mA resulting in a power output 32.41 mW. While it is unexpected that power will be transmitted to the receiver for long periods of time, the aforementioned testing conditions were maintained for a 15 min time period to demonstrate the suitability and power carrying capabilities of the 0.4 mm solid copper wire.

Software application PuTTY [108] was used in tandem with a Raspberry Pi Zero W [109] to allow transmission of the I2C data back to the author's computer over Secure Shell Protocol. The equipment setup is demonstrated in Figure 14.

The metallic elements in the TMP117 module as well as the wiring did not create interference in the magnetic field generated by the high-power transmitter. This was observed through the Rigol DS1054Z Oscilloscope [98], with no change in the CC voltage regardless of the module's presence.

As observed in Figure 15, a strong positive correlation was seen which related wire temperature to time and power. Temperature variance (ΔT) was measured to be 0.242°C, starting at 21.367°C (T_{min}) and ending at 21.609°C (T_{max}).

$$\Delta T = T_{max} - T_{min} \tag{6}$$

The results observed from the experiment highlight the power transmission capacity of the 0.4 mm solid copper wire, with a ΔT of 0.242°C. This temperature fluctuation is deemed negligible, as it remains well under the 2°C threshold at which protein denaturation becomes a risk in the human body [37, 85].

It is to be noted that there are limitations involved with this preliminary testing which do not account for

Figure 14: Temperature sensor setup.

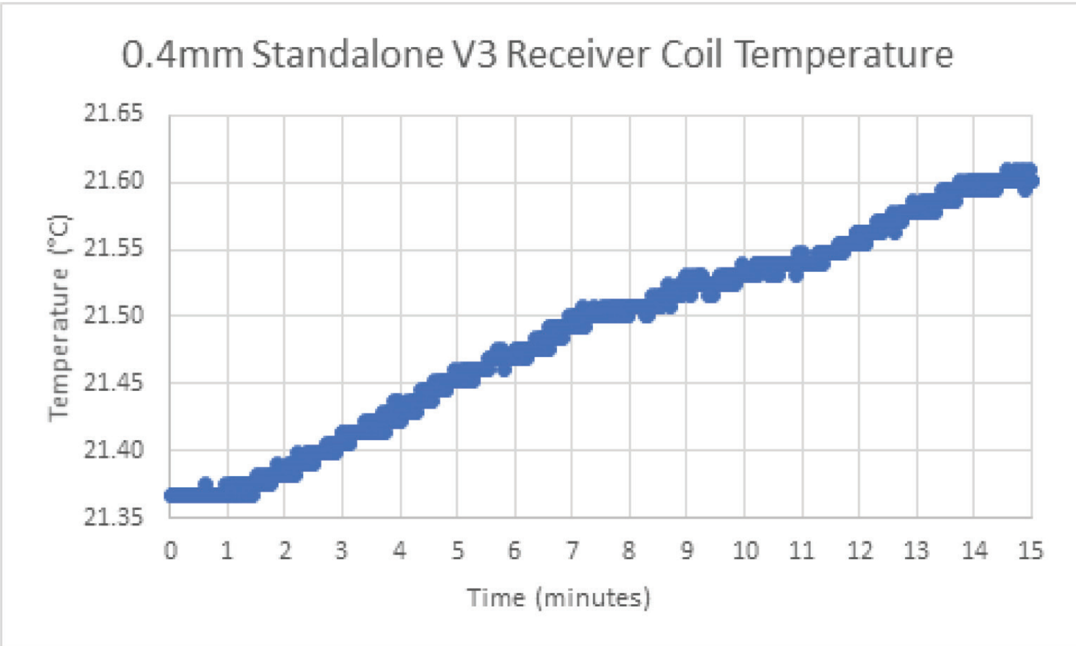

Figure 15: Receiver coil temperature as a function of time.

the coil starting temperature when encased within the human body. It remains unexplored whether the relationship between temperature, power, and time behaves differently if the receiver coil's starting temperature is elevated. Despite this, test conditions involving the delivery of excessive power over an extended time period affirm the attainment of success.

V. Conclusions

Inductive coupling as a form of WPT for deep-situated IMDs encased in tissue and bone was shown to be feasible, following the measures of success outlined before. Three types of receiver coil architectures were explored and designed around the geometry of a PEEK XLIF Nuvasive Coroent XL interbody cage. With the use of off-the-shelf components, functionality was only attainable for the V3 coil design with featured 0.4 mm wire windings around horizontal and verticals beam present on the implant. This design involved manually winding a 0.4 mm wire around every horizontal and vertical beam present on the interbody cage.

Optimized for a 141 kHz working frequency, at a 100 mm coupling distance with a 463.8 Ω DC load attached, it was shown that 1.83 V and 3.94 mA can be induced. Therefore, resulting in a power output of 7.21 mW. Testing was conducted at increased vertical misalignment for outlier patients who required a larger coupling distance between the coils, but this was not realized due to the lack of induced power. Furthermore, vertical misalignment testing occurred through cancellous bone, cortical bone, and adipose tissue substitutes and found that no losses in PTE or PDL were observed.

The effects of angular misalignment were tested and determined that even at small angles such as 15°, PTE and PDL are reduced by up to 34%. As such, the transmitting coil must be kept perfectly aligned to reach the required PDL and PTE. In addition, planar and horizontal misalignment effects were observed. However, these forms of misalignment are easier to resolve and simply require rotating the primary coil or translating the position of the primary coil when parallel to the patient's back.

At decreased coupling distances, biological safety must be considered when regulating voltage for the EFM8BB52 microcontroller. A temperature sensing module using a highly sensitive TMP117 sensor was explored in section 3.9 and can be utilized for testing of this nature. One such example was the testing of the receiver coil resistance to temperature increases. It was observed that for a PDL of 26.43 mA, which greatly exceeds the power requirement for the IMD, the temperature of the receiving coil increased by a negligible factor of 0.242°C over a period of 15 min. Thus, highlighting the power-carrying capabilities of the 0.4 mm solid copper wire.

In addition, LSK as a means of data telemetry was attempted; however, due to a low coupling factor between the primary and secondary coils, it was not realized. As such, this necessitated the requirement for an active means of data transmission. UWB was researched and showed the most promising results, with the power for these active antenna components being the factor in the feasibility analysis.

It is recommended that a custom transmitting coil is developed, alongside circuitry which will power the system. In doing so, a great level of control will be afforded to the system designer and can result in gains in PTE and PDL through impedance matching and working frequency optimization. Furthermore, the inclusion of a steel core in the interbody cage should be explored to increase the coupling factor. Thus, potentially allowing LSK to be used as a form of data transmission.

VI. Patents

A patent has been published as "A Surgical Implant" by the International Application Number WO2022/232861 A1, dated November 10, 2022, by the inventors, V. Ramakrishna, G. Prusty, A. Diwan and S. C. Mukhopadhyay.

Author Contributions

Conceptualization: SM, VR, GP, BG, SM, AD; methodology: VR, IS, SM; software, SM, VR.; validation: IS, VR.; formal analysis: SM, IS, VR, BG.; investigation: IS, VR.; resources: SM; data curation: IS, VR.; writing—original draft preparation: SM, IS.; writing—review and editing: IS, VR, SM, BG, GP, AD.; visualization: IS, VR.; supervision: SM, BG, GP, AD; project administration: SM; funding acquisition: SM, GP. All authors have read and agreed to the published version of the manuscript."

Funding

This research received no external funding.

Conflicts of Interest

The authors declare no conflicts of interest.

References

[1] R. J. Mobbs, K. Phan, G. Malham, K. Seex and P. J. Rao, "Lumbar interbody fusion: techniques, indications and comparison of interbody fusion options including PLIF, TLIF, MI-TLIF, OLIF/ATP, LLIF and ALIF," *Journal of Spine Surgery,* vol. 1, no. 1, p. 2–18, 2015.

[2] D. Hoy, C. Bain, G. Williams, L. March, P. Brooks, F. Blyth, A. Woolf, T. Vos and R. Buchbinder, "A systematic review of the global prevalence of low back pain," *Arthritis and Rheumatism*, vol. 64, no. 6, pp. 2028–2037, 2012.

[3] J. W. Frymoyer, "Back pain and sciata," *The New England Journal of Medicine*, vol. 218, no. 5, pp. 291–300, 1988.

[4] J. B. Dillane, J. Fry and G. Kalton, "Acute Back Syndrome—A Study from General Practice," *BMJ*, vol. 2, no. 5505, pp. 82–84, 1966.

[5] D. K. Resnick, T. F. Choudhri, A. T. Dailey, M. W. Groff, L. Khoo, P. G. Matz, P. Mummaneni, W. C. Watters III, J. Wang, B. C. Walters and M. N. Hadley, "Guidelines for the performance of fusion procedures for degenerative disease of the lumbar spine. Part 7: intractable low-back pain without stenosis or spondylolisthesis," *Journal of Neurosurgery: Spine*, vol. 2, no. 6, pp. 670-672, 2005.

[6] B. I. Martin, S. K. Mirza, N. Spina, W. R. Spiker, B. Lawrence and D. S. Brodke, "Trends in Lumbar Fusion Procedure Rates and Associated Hospital Costs for Degenerative Spinal Diseases in the United States, 2004 to 2015," *Spine*, vol. 44, no. 5, p. 369–376, 2019.

[7] R. A. Deyo, D. Cherkin, D. Conrad and E. Volinn, "Cost, controversy, crisis: low back pain and the health of the public," *Annual Review of Public Health*, vol. 12, no. 1, p. 141–156, 1991.

[8] H. Briggs and P. R. Milligan, "Chip fusion of the low back following exploration of the spinal canal," *The Journal of Bone & Joint Surgery*, vol. 26, no. 1, pp. 125–130, 1944.

[9] B. M. Ozgur, H. E. Aryan, L. Pimenta and W. R. Taylor, "Extreme Lateral Interbody Fusion (XLIF): a novel surgical technique for anterior lumbar interbody fusion," *The Spine Journal*, vol. 6, no. 4, p. 435–443, 2006.

[10] G. M. Malham, N. J. Ellis, R. M. Parker, C. M. Blecher, R. White, B. Goss and K. A. Seex, "Maintenance of segmental lordosis and disk height in stand-alone and instrumented extreme lateral interbody fusion (XLIF)," *Clinical Spine Surgery*, vol. 30, no. 2, pp. 90–98, 2017.

[11] M. Si, J. Guo, J. Hao, X. Zhao, C. A. Randall and H. Wang, "Cold sintered composites consisting of PEEK metal oxides with improved electrical properties via the hybrid interfaces," *Composites. Part B, Engineering*, vol. 226, p. 109349, 2021.

[12] E. Massaad, N. Fatima, A. Kiapour, M. Hadzipasic, G. M. Shankar and J. H. Shin, "Polyetheretherketone Versus Titanium Cages for Posterior Lumbar Interbody Fusion: Meta-Analysis and Review of the Literature," *Neurospine*, vol. 17, no. 1, pp. 125–135, 2020.

[13] M.-C. Kim, H.-T. Chung, J.-L. Cho, D.-J. Kim and N.-S. Chung, "Subsidence of polyetheretherketone cage after minimally invasive transforaminal lumbar interbody fusion," *Journal of Spinal Disorders & Techniques*, vol. 26, no. 2, pp. 87–92, 2013.

[14] F. Galbusera, D. Volkheimer, S. Reitmaier, N. Berger-Roscher, A. Kienle and H.-J. Wilke, "Pedicle screw loosening: a clinically relevant complication?," *European Spine Journal*, vol. 24, no. 5, pp. 1005–1016, 2015.

[15] C. Herren, R. M. Simons, J. Bredow, S. Oikonomidis, L. Westermann, R. Sobottke, M. J. Scheyerer, M. Pishnamaz, P. Eysel, K. Zarghooni, J. Franklin and J. Siewe, "Posterior Lumbar Interbody Fusion versus Dynamic Hybrid Instrumentation: A Prospective Randomized Clinical Trial," *World Neurosurgery*, vol. 117, p. e228–e237, 2018.

[16] D. S. Chun, K. C. Baker and W. K. Hsu, "Lumbar pseudarthrosis: a review of current diagnosis and treatment," *Neurosurgical Focus*, vol. 39, no. 4, p. E10, 2015.

[17] P. Berjano, F. Langella, M. Damilano, M. Pejrona, J. Buric, M. Ismael, J. H. Villafañe and C. Lamartina, "Fusion rate following extreme lateral lumbar interbody fusion," *European Spine Journal*, vol. 24, pp. 369–371, 2015.

[18] B. Meng, J. Bunch, D. Burton and J. Wang, "Lumbar interbody fusion: recent advances in surgical techniques and bone healing strategies," *European Spine Journal*, vol. 30, no. 1, pp. 22-33, 2021.

[19] W. K. Hsu, M. S. Nickoli, J. C. Wang, J. R. Lieberman, H. S. An, S. T. Yoon, J. A. Youssef, D. S. Brodke and C. M. McCullough, "Improving the Clinical Evidence of Bone Graft Substitute Technology in Lumbar Spine Surgery," *Global Spine Journal*, vol. 2, no. 4, p. 239–248, 2012.

[20] E. Klineberg, M. Gupta, I. McCarthy and R. Hostin, "Detection of Pseudarthrosis in Adult Spinal Deformity: The Use of Health-related Quality-of-life Outcomes to Predict Pseudarthrosis,"

Clinical Spine Surgery, vol. 29, no. 8, pp. 318-322, 2016.

[21] L. Y. Carreon, S. D. Glassman, J. D. Schwender, B. R. Subach, M. F. Gornet and S. Ohno, "Reliability and accuracy of fine-cut computed tomography scans to determine the status of anterior interbody fusions with metallic cages," *Spine Journal*, vol. 8, no. 6, pp. 998-1002, 2018.

[22] M. Mujeeb-U-Rahman, D. Adalian, C.-F. Chang and A. Scherer, "Optical power transfer and communication methods for wireless implantable sensing platforms," *Journal of Biomedical Optics*, vol. 20, no. 9, pp. 095012:1 - 095012:9, 2015.

[23] Anindya Nag, Subhas Chandra Mukhopadhyay, Flexible Sensors for Energy-Harvesting Applications, Springer-Nature, Vol. 42, 2022.

[24] P. Cinquin, C. Gondran, F. Giroud, S. Mazabrard, A. Pellissier, F. Boucher, J.-P. Alcaraz, K. Gorgy, F. Lenouvel, S. Mathé, P. Porcu, S. Cosnier and R. Haverkamp, "A Glucose BioFuel Cell Implanted in Rats," *PLoS ONE*, vol. 5, no. 5, p. e10476, 2010.

[25] B. Shi, Z. Li and Y. Fan, "Implantable Energy-Harvesting Devices," *Advanced Materials*, vol. 30, no. 44, pp. 1801511-1801529, 2018.

[26] H. A. Owida, J. I. Al-Nabulsi, N. M. Turab, F. Alnaimat, H. Rababah, M. Y. Shakour, C. Galli and C. Galli, "Autocharging Techniques for Implantable Medical Applications," *International Journal of Biomaterials*, vol. 2021, pp. 1-7, 2021.

[27] D. H. Kim, H. J. Shin, H. Lee, C. K. Jeong, H. Park, G. Hwang, H. Lee, D. J. Joe, J. H. Han, S. H. Lee, J. Kim, B. Joung and K. J. Lee, "In Vivo Self-Powered Wireless Transmission Using Biocompatible Flexible Energy Harvesters," *Advanced Function Materials*, vol. 27, no. 25, p. 1700341, 2017.

[28] O. V. Gorskii, "Potential Power Supply Methods for Implanted Devices," *Biomedical Engineering*, vol. 52, no. 3, p. 204–209, 2018.

[29] S. R. Khan, S. K. Pavuluri, G. Cummins and M. P. Y. Desmulliez, "Wireless Power Transfer Techniques for Implantable Medical Devices: A Review," *Sensors*, vol. 20, no. 12, pp. 1-58, 2020.

[30] A. B. Amar, A. B. Kouki and H. Cao, "Power approaches for implantable medical devices," *Sensors*, vol. 15, no. 11, p. 28889–28914, 2015.

[31] Chinthaka Pasan Gooneratne, Subhas Mukhopadhyay, Bodong Li, Guodong Zhan, Arturo Magana-Mora, Timothy Eric Moellendick, Triboelectric energy harvesting with pipe-in-pipe structure, US Patent, number 11,421,513, 2022.

[32] J. Li, L. Kang, Y. Long, H. Wei, Y. Yu, Y. Wang, C. A. Ferreira, G. Yao, Z. Zhang, C. Carlos, L. German, X. Lan, W. Cai and X. Wang, "Implanted Battery-Free Direct-Current Micro-Power Supply from in Vivo Breath Energy Harvesting," *ACS Applied Materials & Interfaces*, vol. 10, no. 49, pp. 42030-42038, 2018.

[33] C. K. Jeong, K. M. Baek, S. Niu, T. W. Nam, Y. H. Hur, D. Y. Park, G.-T. Hwang, M. Byun, Z. L. Wang, Y. S. Jung and K. J. Lee, "Topographically-Designed Triboelectric Nanogenerator via Block Copolymer Self-Assembly," *Nano Letters*, vol. 14, no. 12, p. 7031–7038, 2014.

[34] S. El Ichi-Ribault, J.-P. Alcaraz, F. Boucher, B. Boutaud, R. Dalmolin, J. Boutonnat, P. Cinquin, A. Zebda and D. K. Martin, "Remote wireless control of an enzymatic biofuel cell implanted in a rabbit for 2 months," *Electrochimica Acta*, vol. 269, pp. 360-366, 2018.

[35] A. Pfenniger, M. Jonsson, A. Zurbuchen, V. M. Koch and R. Vogel, "Energy Harvesting from the Cardiovascular System, or How to Get a Little Help from Yourself," *Annals of Biomedical Engineering*, vol. 41, no. 11, p. 2248–2263, 2013.

[36] A. Haeberlin, A. Zurbuchen, J. Schaerer, J. Wagner, S. Walpen, C. Huber, H. Haeberlin, J. Fuhrer and R. Vogel, "Successful pacing using a batteryless sunlight-powered pacemaker," *Europace*, vol. 16, no. 10, p. 1534–1539, 2014.

[37] K. Goto, T. Nakagawa, O. Nakamura and S. Kawata, "An Implantable Power Supply with an Optically Rechargeable Lithium Battery," *IEEE Transactions on Biomedical Engineering*, vol. 48, no. 7, p. 830–833, 2001.

[38] J. Kim, J. Seo, D. Jung, T. Lee, H. Ju, J. Han, N. Kim, J. Jeong, S. Cho, J. H. Seol and J. Lee, "Active photonic wireless power transfer into live tissues," *Proceedings of the National Academy of Sciences - PNAS*, vol. 117, no. 29, p. 16856–16863, 2020.

[39] M. P. Theodoridis, "Effective Capacitive Power Transfer," *IEEE Transactions on Power Electronics*, vol. 27, no. 12, pp. 4906-4913, 2012.

[40] A. M. Sodagar and P. Amiri, "Capacitive coupling for power and data telemetry to implantable biomedical microsystems," *2009 4th International IEEE/EMBS Conference on Neural Engineering, 2009*, pp. 411-414, 2009.

[41] K. Detka and K. Gorecki, "Wireless Power Transfer - A Review," *Energies*, vol. 15, no. 19, p. 7236, 2022.

[42] S. Nag, A. Koruprolu, S. M. Saikh, R. Erfani and P. Mohseni, "Auto-Resonant Tuning for Capacitive Power and Data Telemetry Using Flexible Patches," *IEEE Transactions on Circuits and Systems. II, Express Briefs*, vol. 67, no. 10, p. 1804–1808, 2020.

[43] A. Hassan, C. Sawma, M. Hasanuzzaman, B. Gosselin and M. Sawan, "Spatial carrier position modulation based multichannel capacitive link for bioelectronic implants," *2015 IEEE Biomedical Circuits and Systems Conference (BioCAS)*, pp. 1-4, 2015.

[44] G. L. Barbruni, P. M. Ros, D. Demarchi, S. Carrara and D. Ghezzi, "Miniaturised Wireless Power Transfer Systems for Neurostimulation: A Review," *IEEE Transactions on Biomedical Circuits and Systems*, vol. 14, no. 6, p. 1160–1178, 2020.

[45] J. C. Schuder, "Powering an Artificial Heart: Birth of the Inductively Coupled-Radio Frequency System in 1960," *Artificial Organs*, vol. 26, no. 11, pp. 909-915, 2002.

[46] M. C. Edwards, J. M. Hoy, S. I. FitzGibbon and P. J. Murray, "Monitoring with microchips: Microchip-automated doors as a potential novel method for tracking the survival of released Northern Brown Bandicoots," *Ecological Management & Restoration*, vol. 21, no. 3, p. 254–256, 2020.

[47] M. Kiani, U.-M. Jow and M. Ghovanloo, "Design and Optimization of a 3-Coil Inductive Link for Efficient Wireless Power Transmission," *IEEE Transactions on Biomedical Circuits and Systems*, vol. 5, no. 6, p. 579–591, 2011.

[48] U.-M. Jow and M. Ghovanloo, "Design and Optimization of Printed Spiral Coils for Efficient Transcutaneous Inductive Power Transmission," *IEEE Transactions on Biomedical Circuits and Systems*, vol. 1, no. 3, pp. 193-202, 2007.

[49] A. Denisov and E. Yeatman, "Ultrasonic vs. Inductive Power Delivery for Miniature Biomedical Implants," *2010 International Conference on Body Sensor Networks*, pp. 84-89, 2010.

[50] G. Lazzi, "Thermal effects of bioimplants," *IEEE Engineering in Medicine and Biology Magazine*, vol. 24, no. 5, pp. 75-81, 2005.

[51] S. A. Mirbozorgi, P. Yeon and M. Ghovanloo, "Robust Wireless Power Transmission to mm-Sized Free-Floating Distributed Implants," *IEEE Transactions on Biomedical Circuits and Systems*, vol. 11, no. 3, pp. 692-702, 2017.

[52] M. Baker and R. Sarpeshkar, "Feedback Analysis and Design of RF Power Links for Low-Power Bionic Systems," *IEEE Transactions on Biomedical Circuits and Systems*, vol. 1, no. 1, p. 28–38, 2007.

[53] P. Feng, P. Yeon, Y. Cheng, M. Ghovanloo and T. G. Constandinou, "Chip-Scale Coils for Millimeter-Sized Bio-Implants," *IEEE Transactions on Biomedical Circuits and Systems*, vol. 12, no. 5, p. 1088–1099, 2018.

[54] S. R. Khan, S. K. Pavuluri, G. Cummins and M. P. Y. Desmulliez, "Miniaturized 3-D Cross-Type Receiver for Wirelessly Powered Capsule Endoscopy," *IEEE Transactions on Microwave Theory and Techniques*, vol. 67, no. 5, p. 1985–1993, 2019.

[55] B. Lenaerts and R. Puers, "An inductive power link for a wireless endoscope," *Biosensors & Bioelectronics*, vol. 22, no. 7, p. 1390–1395, 2007.

[56] S. Ozeri, D. Shmilovitz, S. Singer and C.-C. Wang, "Ultrasonic transcutaneous energy transfer using a continuous wave 650 kHz Gaussian shaded transmitter," *Ultrasonics*, vol. 50, no. 7, pp. 666-674, 2010.

[57] H. Basaeri, D. B. Christensen and S. Roundy, "A review of acoustic power transfer for bio-medical implants," *Smart Materials and Structures*, vol. 25, no. 12, p. 123001, 2016.

[58] S. Ozeri and D. Shmilovitz, "Ultrasonic transcutaneous energy transfer for powering implanted devices," *Ultrasonics*, vol. 50, no. 6, pp. 556-566, 2010.

[59] M. Meng and M. Kiani, "Design and Optimization of Ultrasonic Wireless Power Transmission Links for Millimeter-Sized Biomedical Implants," *IEEE Transactions on Biomedical Circuits and Systems*, vol. 11, no. 1, pp. 98-107, 2017.

[60] C. Wang, Q. Shi and C. Lee, "Advanced Implantable Biomedical Devices Enabled by Triboelectric Nanogenerators," *Nanomaterials*, vol. 12, no. 8, p. 1366, 2022.

[61] S. Arra, J. Leskinen, J. Heikkila and J. Vanhala, "Ultrasonic Power and Data Link for Wireless Implantable Applications," *2007 2nd International Symposium on Wireless Pervasive Computing*, 2007.

[62] B. L. Turner, S. Senevirathne, K. Kilgour, D. McArt, M. Biggs, S. Menegatti and M. A. Daniele, "Ultrasound-Powered Implants: A Critical Review of Piezoelectric Material Selection and Applications," *Advanced Healthcare Materials*, vol. 10, no. 17, p. 2100986, 2021.

[63] B. M. G. Rosa and G.-Z. Yang, "Ultrasound Powered Implants: Design, Performance Considerations and Simulation Results," *Scientific Reports*, vol. 10, no. 1, p. 6537, 2020.

[64] C. Chen, Z. Wen, J. Shi, X. Jian, P. Li, J. T. W. Yeow and X. Sun, "Micro triboelectric ultrasonic device for acoustic energy transfer and signal communication," *Nature Communications*, vol. 11, no. 1, p. 4143, 2020.

[65] S. Sherrit, M. Badescu, X. Bao, Y. Bar-Cohen and Z. Chang, "Efficient electromechanical network

model for wireless acoustic-electric feed-throughs," *SPIE*, vol. 5758, p. 362–372, 2005.

[66] M. Acosta, N. Novak, V. Rojas, S. Patel, R. Vaish, J. Koruza, G. A. Rossetti and J. Rödel, "BaTiO3-based piezoelectrics: Fundamentals, current status, and perspectives," *Applied Physics Reviews*, vol. 4, no. 4, p. 041305, 2017.

[67] J. Charthad, M. J. Weber, T. C. Chang and A. Arbabian, "A mm-Sized Implantable Medical Device (IMD) With Ultrasonic Power Transfer and a Hybrid Bi-Directional Data Link," *IEEE Journal of Solid-State Circuits*, vol. 50, no. 8, p. 1741–1753, 2015.

[68] C. Li, K.-F. Un, P.-i. Mak, Y. Chen, J.-M. Munoz-Ferreras, Z. Yang and R. Gomez-Garcia, "Overview of Recent Development on Wireless Sensing Circuits and Systems for Healthcare and Biomedical Applications," *IEEE Journal on Emerging and Selected Topics in Circuits and Systems*, vol. 8, no. 2, p. 165–177, 2018.

[69] M. J. Weber, Y. Yoshihara, A. Sawaby, J. Charthad, T. C. Chang and A. Arbabian, "A Miniaturized Single-Transducer Implantable Pressure Sensor With Time-Multiplexed Ultrasonic Data and Power Links," *IEEE Journal of Solid-State Circuits*, vol. 53, no. 4, p. 1089–1101, 2018.

[70] R. Hinchet, H.-J. Yoon, H. Ryu, M.-K. Kim, E.-K. Choi, D.-S. Kim and S.-W. Kim, "Transcutaneous ultrasound energy harvesting using capacitive triboelectric technology'," *Science (American Association for the Advancement of Science)*, vol. 365, no. 6452, p. 491–494, 2019.

[71] G. Jiang, "Design challenges of implantable pressure monitoring system," *Frontiers in Neuroscience*, vol. 4, p. 29, 2010.

[72] T. Dong, Y. Gu, T. Liu and M. Pecht, "Resistive and capacitive strain sensors based on customized compliant electrode: Comparison and their wearable applications," *Sensors and Actuators A: Physical*, vol. 326, p. 112720, 2021.

[73] N. Arfah, A. H. M. Z. Alam and S. Khan, "Capacitance-to-voltage converter for capacitance measuring system," *2011 4th International Conference on Mechatronics (ICOM)*, pp. 1-4, 2011.

[74] C. Zhang, R. Gallichan, D. M. Budgett and D. McCormick, "A capacitive pressure sensor interface ic with wireless power and data transfer," *Micromachines*, vol. 11, no. 10, p. 897, 2020.

[75] Z. Ma, Y. Zhang, K. Zhang, H. Deng and Q. Fu, "Recent progress in flexible capacitive sensors: Structures and properties," *Nano Materials Science*, 2022.

[76] M. Cicalini, M. Piotto, P. Bruschi and M. Dei, "Design of a Capacitance-to-Digital Converter Based on Iterative Delay-Chain Discharge in 180 nm CMOS Technology," *Sensors*, vol. 22, no. 1, p. 121, 2021.

[77] R. Wei, W. Wang, X. Xiao and Q. Chen, "A Low-Power Delta-Sigma Capacitance-to-Digital Converter for Capacitive Sensors," *IEEE Access*, vol. 7, p. 78281–78288, 2019.

[78] Prashanth V. and George B., "An Improved Capacitance-to-digital Converter for Leaky Capacitive sensors", IEEE Sensors Journal, vol. 15, no. 11, pp. 6238-6247, Nov. 2015.

[79] Sreenath V. and George B., "An Improved Closed-Loop Switched Capacitor Capacitance to Frequency Converter and Its Evaluation", IEEE Transactions on Instrumentation and Measurement, vol. 67, no. 5, pp. 1028-1035, May 2018.

[80] B. Lee and M. Ghovanloo, "An Overview of Data Telemetry in Inductively Powered Implantable Biomedical Devices," *IEEE Communications Magazine*, vol. 57, no. 2, p. 74–80, 2019.

[81] S. Ha, C. Kim, J. Park, S. Joshi and G. Cauwenberghs, "Energy Recycling Telemetry IC With Simultaneous 11.5 mW Power and 6.78 Mb/s Backward Data Delivery Over a Single 13.56 MHz Inductive Link," *IEEE Journal of Solid-State Circuits*, vol. 51, no. 11, p. 2664–2678, 2016.

[82] Vivek AS Ramakrishna, Uphar Chamoli, Subhas C Mukhopadhyay, Ashish D Diwan, B Gangadhara Prusty, Measuring compressive loads on a 'smart'lumbar interbody fusion cage: Proof of concept, Journal of Biomechanics, Elsevier, vol. 147, pp. 111440, 2023.

[83] A. Ebrazeh and P. Mohseni, "30 pJ/b, 67 Mbps, Centimeter-to-Meter Range Data Telemetry With an IR-UWB Wireless Link," *IEEE Transactions on Biomedical Circuits and Systems*, vol. 9, no. 3, p. 362–369, 2015.

[84] J. M. Anderson, "Inflammatory Response to Implants," *ASAIO Journal*, vol. 34, no. 2, p. 101–107, 1988.

[85] P. D. Wolf and W. M. Reichert, "Thermal Considerations for the Design of an Implanted Cortical Brain–Machine Interface (BMI)," in *Indwelling Neural Implants*, CRC Press, 2008, pp. 81-104.

[86] C. R. Davies, F. Fukumura, K. Fukamachi, K. Muramoto, S. C. Himley, A. Massiello, J.-F. Chen and H. Harasaki, "Adaptation of tissue to a chronic heat load," *ASAIO Journal*, vol. 40, no. 3, p. M514–M517, 1994.

[87] D. Jiang, B. Shi, H. Ouyang, Y. Fan, Z. L. Wang and Z. Li, “Emerging Implantable Energy Harvesters and Self-Powered Implantable Medical Electronics,” *ACS Nano*, vol. 14, no. 6, p. 6436–6448, 2020.

[88] K. N. Bocan and E. Sejdić, “Adaptive transcutaneous power transfer to implantable devices: A state of the art review,” *Sensors*, vol. 16, no. 3, p. 393, 2016.

[89] T. Laube, C. Brockmann, R. Buss, C. Lau, K. Höck, N. Stawski, T. Stieglitz, H. A. Richter and H. Schilling, “Optical energy transfer for intraocular microsystems studied in rabbits,” *Graefe’s Archive for Clinical and Experimental Ophthalmology*, vol. 242, no. 8, p. 661–667, 2004.

[90] X. Zhuang, A. Nikoozadeh, M. A. Beasley, G. G. Yaralioglu, B. T. Khuri-Yakub and B. L. Pruitt, “Biocompatible coatings for CMUTs in a harsh, aqueous environment,” *Journal of Micromechanics and Microengineering*, vol. 17, no. 5, p. 994–1001, 2007.

[91] D. S. Lee, S. J. Kim, E. B. Kwon, C. W. Park, S. M. Jun, B. Choi and S. W. Kim, “Comparison of in vivo biocompatibilities between parylene-C and polydimethylsiloxane for implantable microelectronic devices,” *Bulletin of Materials Science*, vol. 36, no. 6, p. 1127–1132, 2013.

[92] A. Ibrahim, M. Meng and M. Kiani, “A Comprehensive Comparative Study on Inductive and Ultrasonic Wireless Power Transmission to Biomedical Implants,” *IEEE Sensors Journal*, vol. 18, no. 9, p. 3813–3826, 2018.

[93] M. O. Culjat, D. Goldenberg, P. Tewari and R. S. Singh, “A Review of Tissue Substitutes for Ultrasound Imaging,” *Ultrasound in Medicine & Biology*, vol. 36, no. 6, p. 861–873, 2010.

[94] Silicon Labs, “EFM8BB52 Data Sheet,” Silicon Labs, 2021. [Online]. Available: https://www.silabs.com/documents/public/data-sheets/efm8bb52-datasheet.pdf. [Accessed 8 June 2023].

[95] Amphenol, “P122 High Silicon Pressure Sensor Die,” Amphenol, 2018. [Online]. Available: https://www.amphenol-sensors.com/en/novasensor/pressure-sensor-die/3166-p122. [Accessed 11 November 2022].

[96] NuVasive, “Coroent Thoracolumbar System Patient Information Leaflet,” NuVasive, 1 December 2021. [Online]. Available: https://www.nuvasive.com/wp-content/uploads/2021/11/CoRoent-Thoracolumbar-System-Patient-Information-Leaflet_Final.pdf. [Accessed 12 June 2023].

[97] PTC, “Creo Parametric 3D Modelling Software,” PTC, 2023. [Online]. Available: https://www.ptc.com/en/products/creo/parametric. [Accessed 12 June 2023].

[98] Chinthaka Pasan Gooneratne, Subhas Mukhopadhyay, Bodong Li, Guodong Zhan, Arturo Magana-Mora and Timothy Eric Moellendick, Triboelectric energy harvesting with pipe-in-pipe structure, US Patent 11,421,513, 2022.

[99] Keysight Technologies, “U1730C Series Handheld LCR Meters,” Keysight Technologies, 18 October 2018. [Online]. Available: https://www.keysight.com/au/en/assets/7018-02950/data-sheets/5990-7778.pdf. [Accessed 12 June 2023].

[100] Onsemi, “1N5820, 1N5821, 1N5822 - Axial Lead Rectifiers,” Onsemi, December 2007. [Online]. Available: https://www.onsemi.com/pdf/datasheet/1n5820-d.pdf. [Accessed 10 June 2023].

[101] J. Harries, T. H. Jochimsen, T. Scholz, T. Schlender, H. Barthel, O. Sabri and B. Sattler, “A realistic phantom of the human head for PET-MRI,” *EJNMMI Physics*, vol. 7, no. 1, p. 52, 2020.

[102] Nguyen Thi Phuoc Van, Syed Faraz Hasan, Xiang Gui, Subhas Mukhopadhyay, Hung Tran, Three-step two-way decode and forward relay with energy harvesting, IEEE Communications Letters, Vol. 21, Issue 4, pp. 857-860, 2016.

[103] Vivek AS Ramakrishna, Uphar Chamoli, Alessandro G Larosa, Subhas C Mukhopadhyay, B Gangadhara Prusty, Ashish D Diwan, A biomechanical comparison of posterior fixation approaches in lumbar fusion using computed tomography based lumbosacral spine modelling, Proceedings of the Institution of Mechanical Engineers, Part H: Journal of Engineering in Medicine, SAGE Publishing, vol. 237, Issue 2, pp. 243-253, 2023.

[104] H. E. Jaramillo, L. Gómez and J. J. García, “A finite element model of the L4-L5-S1 human spine segment including the heterogeneity and anisotropy of the discs,” *Acta of Bioengineering and Biomechanics*, vol. 17, no. 2, p. 15–24, 2015.

[105] Texas Instruments, “TMP117 High-Accuracy, Low-Power, Digital Temperature Sensor With SMBus™ - and I2C-Compatible Interface,” Texas Instruments, September 2022. [Online]. Available: https://www.ti.com/lit/ds/symlink/tmp117.pdf?ts=1668131690221. [Accessed 11 November 2022].

[106] Core Electronics, “PiicoDev Precision Temperature Sensor TMP117,” Core Electronics, 2023. [Online]. Available: https://core-electronics.com.au/piicodev-precision-temperature-sensor-tmp117.html. [Accessed 6 June 2023].

[107] Python, “Python Programing Language,” Python, 2023. [Online]. Available: https://www.python.org/. [Accessed 6 June 2023].

[108] PuTTY, "PuTTY Program," PuTTY, 2023. [Online]. Available: https://www.putty.org/. [Accessed 6 June 2023].

[109] Raspberry Pi, "Raspberry Pi Zero W," Raspberry Pi, 2023. [Online]. Available: https://www.raspberrypi.com/products/raspberry-pi-zero-w/. [Accessed 6 June 2023].

[110] J. P. Sanjurjo, E. Prefasi, C. Buffa and R. Gaggl, "A Capacitance-To-Digital Converter for MEMS Sensors for Smart Applications," *Sensors*, vol. 17, no. 6, p. 1312, 2017.

[111] Z. Tan, H. Jiang, H. Zhang, X. Tang, H. Xin and S. Nihtianov, "Power-Efficiency Evolution of Capacitive Sensor Interfaces," *IEEE Sensors Journal*, vol. 21, no. 11, p. 12457–12468, 2021.

[112] Rectron Semiconductor, "Single-Phase Silicon Bridge Rectifier BR1005 Thru BR1010," Rectron Semiconductor, May 2001. [Online]. Available: https://www.jaycar.com.au/medias/sys_master/images/images/9965579567134/ZR1320-dataSheetMain.pdf. [Accessed 6 June 2023].

[113] F. Durmus and S. Karagol, "Mutual Inductance Calculation for Planar Square and Hexagonal Coils," *Arabian Journal for Science and Engineering*, vol. 47, no. 3, p. 3409–3420, 2022.

[114] Vivek AS Ramakrishna, Uphar Chamoli, Alessandro G Larosa, Subhas C Mukhopadhyay, B Gangadhara Prusty, Ashish D Diwan, Finite element modeling of temporal bone graft changes in XLIF: Quantifying biomechanical effects at adjacent levels, Journal of Orthopaedic Research®, Vol. 40, Issue, 6, pp. 1420-1435, 2022.

[115] Keysight Technologies, "N2791A 25 MHz High Voltage Differential Probe," Keysight Technologies, 13 September 2021. [Online]. Available: https://www.keysight.com/au/en/assets/7018-02105/data-sheets/5990-3780.pdf. [Accessed 10 June 2023].

[116] Gunjan Gupta and Robert Van ZylEnergy harvested end nodes and performance improvement of LoRa networks, International Journal on Smart Sensing and Intelligent Systems, VOLUME 14 (2021): ISSUE 1 (JANUARY 2021), Mar 01, 202, 15 pages, DOI: DOI: 10.21307/ijssis-2021-002.

[117] M. Tanaka, S. Sonawane, Y. Fujiwara, K. Uotani, T. Yamauchi, T. Omori and K. Hashizume, "Surgical treatment for spondyloptosis: A case report," *Interdisciplinary Neurosurgery : Advanced Techniques and Case Management*, vol. 25, p. 101161, 2021.

[118] H. J. Kim, V. Nemani, O. Boachie-Adjei, M. E. Cunningham, J. A. Iorio, K. O'Neill, B. J. Neuman and L. G. Lenke, "Distal Fusion Level Selection in Scheuermann's Kyphosis: A Comparison of Lordotic Disc Segment Versus the Sagittal Stable Vertebrae," *Global Spine Journal*, vol. 7, no. 3, p. 254–259, 2017.

[119] M. S. Park, S.-H. Moon, T.-H. Kim, J. K. Oh, H. J. Kang and K. D. Riew, "Radiographic Comparison between Cervical Spine Lateral and Whole-Spine Lateral Standing Radiographs," *Global Spine Journal*, vol. 6, no. 2, p. 118–123, 2016.

[120] International Organization for Standardization, "ISO 10993-1:2018," International Organization for Standardization, October 2018. [Online]. Available: https://www.iso.org/standard/68936.html. [Accessed 12 June 2023].

[121] Keysight Technologies, "U1230 Series - Handheld Digital Multimeteres," Keysight Technologies, 22 February 2022. [Online]. Available: https://www.keysight.com/au/en/assets/7018-02915/data-sheets/5990-7550.pdf. [Accessed 12 June 2023].